

Charged lithium adsorption on pristine and defective silicene: a theoretical study

Julián Juan¹, Luciana Fernández-Werner², Pablo Bechthold¹,
Julián Villarreal¹, Francisco Gaztañaga¹, Paula V Jasen^{1,*},
Ricardo Faccio² and Estela A González¹

¹ Instituto de Física del Sur (IFISUR), Departamento de Física, Universidad Nacional del Sur (UNS), CONICET, Av. L. N. Alem 1253, B8000CPB-Bahía Blanca, Argentina

² Área Física and Centro NanoMat, DETEMA, Facultad de Química, Universidad de la República, Montevideo, Uruguay

E-mail: pjasen@uns.edu.ar

Received 28 January 2022, revised 25 March 2022

Accepted for publication 31 March 2022

Published 14 April 2022



Abstract

We investigated by first principle calculations the adsorption of Li^q ($q = -1, 0$ or $+1$) on a silicene single layer. Pristine and three different defective silicene configurations with and without Li doping were studied: single vacancy (SV), double vacancy (DV) and Stone–Wales (STW). Structural studies and the adsorption energies of various sites were obtained and compared in order to understand the stability of the Li on the surface. Moreover, electronic structure and charge density difference analysis were performed before and after adsorption at the most stable sites, which showed the presence of a magnetic moment in the undoped SV system, the displacement of the Fermi level produced by Li doping and a charge transfer from Li to the surface. Additionally, quantum capacity (QC) and charge density studies were performed on these systems. This analysis showed that the generation of defects and doping improves the QC of silicene in positive bias, because of the existence of 3p orbital in the zone of the defect. Consequently, the innovative calculations performed in this work of charged lithium doping on silicene can be used for future comparison with experimental studies of this Li-ion battery anode material candidate.

Keywords: silicene, defect, lithium, charged Li-ion, DFT

 Supplementary material for this article is available [online](#)

(Some figures may appear in colour only in the online journal)

1. Introduction

The discovery of graphene has motivated theoretical and experimental research toward the synthesis of other analogous 2D materials such as hexagonal boron nitride (h-BN), Xenes ($X = \text{Si}, \text{Ge}, \text{Sb}, \text{etc}$) and molybdenum disulfide (MoS_2), among others. 2D materials have a wide surface and have unique electronic properties as compared to bulk materials. Because of their high surface–volume ratio, these materials are applicable for high charging capacity and long cycle life for metal-ion batteries [1]. Furthermore, the multifunctionality

characteristics of these materials are also one of the main reasons they have received attention from researchers. Due to the high stability, high abundance, and the existence of an excellent compatible oxide, Si and Si-based layered materials are the leading ones for microelectronic devices and may be the most promising materials for realistic applications [2, 3]. In the large family of 2D materials, silicene deserves a special consideration because of its compatibility and expected integration with current nanotechnology. Silicene is a silicon counterpart of graphene with a tiny band gap of 1.55 meV [4]. Takeda and Shiraishi have already reported a 2D graphite-like structure for Si and Ge as a theoretical possibility in 1994 [5]

* Author to whom any correspondence should be addressed.

but the term ‘silicene’ was first introduced by Guzmán-Verri and Lew Yan Voon in 2007 [6]. Nonetheless, it was not until 2012 that silicene was experimentally synthesized and fulfilled the theoretical prediction of the silicene monolayer [7–10].

In contrast to graphene, silicene cannot exist in freestanding form and needs to be grown on a substrate, but cannot be exfoliated from it. Moreover, this honeycomb structure needs an sp^3 substrate due to its tendency toward hybridization [4]. The synthesis of silicene was achieved successfully on a variety of substrates such as metal surfaces [9–18], conductive ceramics [10], h-BN [19], MoS_2 [20], $CaSi_2$ [21], AlN [22] and semi-conducting substrates [23]. Recent progress in the growth of silicene and germanene has been summarized by Kaloni *et al* [24]. Silicene displays several remarkable properties arising from its hexagonal symmetry and Dirac cone structure, e.g., high charge carrier mobility [25] and excellent optical absorption [26]. The low buckling is a consequence of the mixed sp^2 – sp^3 hybridizations of silicon atoms [27]. This allows silicene to surpass graphene in some aspects; including greater spin–orbit coupling (SOC), quantum spin Hall effect, more accessible tunability of the band gap and stronger valley polarization among others related properties [28–30]. These characteristics have made silicene a candidate for various areas of application including field-effect transistors (FET) [16, 31], alkali metal-batteries [32–36], spintronic and valleytronic devices [37], sensors [38], among others. Several reviews are dedicated to the state of art of silicene as well as other 2D materials beyond graphene and their device and technological applications [1, 4, 13, 27, 39–46]. Nonetheless, because of experimental complexities, theoretical studies can be considered as an alternative in order to evaluate the application prospect. It is well known that the adsorption of alkali metal atoms [32–36, 47], transition metal atoms [47–49] or chemical groups [50] provides various ways to modify the structural, electronic, optoelectronic and magnetic properties of 2D materials. Lithium-ion batteries (LIBs) have become the most successful type of energy-storage device for applications ranging from portable electronic devices such as smartphones and laptop computers, to modes of transport such as electric vehicles (EVs), due to their lightweight, environmental friendliness, and high energy density [51]. So, the demand for portable energy sources is currently increasing and improvements in LIBs have become an important quest. The conventional material used as the anode is graphite but a new alternative is the 2D graphene-like forms such as silicene. Therefore, understanding the formation and migration of defects as well as their influences on the electronic/magnetic properties of these novel 2D materials not only is meaningful for fundamental research, but also provides a powerful route to tailor their physical properties and to control their functional applications in future devices.

Silicene has the distinctive property of a buckled honeycomb structure, allowing better interactions of this surface with Li atoms, and therefore advantageous for application in Li-ion batteries. Theoretical studies have recently been performed regarding the adsorption and diffusion of Li on pristine silicene without substrate [33–36, 51–60]. Tritsarlis *et al* [52]

performed first-principles calculations to investigate the interaction of Li with Si in model electrodes of freestanding single-layer and double-layer silicene. The authors identified strong binding sites for Li and calculated the energy barriers accompanying Li diffusion. They reported a binding energy of Li of ~ 2.2 eV per Li atom and show small variation with respect to Li content and silicene thickness (one or two layers) while the barriers for Li diffusion are relatively low, typically less than 0.6 eV. Osborn and Farajian [53] explored the nature of the interaction between lithium and silicene. The authors assess the energetics and stability of partially and fully lithiated silicene via structure optimization and molecular dynamics (MD) simulations based on DFT. Subsequently, they explore the electronic and phononic characteristics of the stable lithiated silicene. Their results show that, like hydrogenated silicene, lithiated silicene is more stable, relative to its bulk counterpart, than bare silicene. The stability of the fully lithiated case was further verified by molecular dynamics at 300 and 900 K and phonon frequency calculations. The band structure of silicene changes from a zero-gap to a 0.368 eV band-gap semiconductor for complete lithium adsorption. Lithiation could provide a unique way of isolating silicene while inducing and tuning its band gap. Huang *et al* [59] studied the adsorption and diffusion of Li on silicene using DFT. Their calculated results show that the adsorption energy of Li on silicene is larger than that of Li on graphene, and it increases with the increasing concentration of Li adatoms. Low diffusion energy barrier of Li on silicene, regardless of the concentration of adsorbed atoms, means that the silicene is a suitable material for future anodes of LIBs. Seyed-Talebi *et al* [60] performed DFT calculations to study the adsorption mechanism of Li metal atom and Li-ion onto freestanding silicene (buckled, $\theta = 101.7^\circ$) and compared the results with those of graphene. In both cases the authors used a supercell model. The authors reported that Li adsorption modifies the DOS around the Fermi energy and additional peaks appear in the DOS spectrum and turns silicene into a narrow gap semiconductor. They found that the maximum energy barrier for the migration of Li/Li⁺ adatom on silicene sides is only 1.70/1.75 eV. Low energy barrier implies that Li adatoms can easily penetrate into bilayer or multilayer silicene.

During the fabrication and processing of silicene monolayers, structural defects are almost inevitable. Setiadi *et al* [56] performed DFT calculations of the defect formation energies in silicene, the binding of Li atoms to these defects, and its diffusion across and through silicene. They focused on the single vacancy (SV), double-vacancy (DV) and Stone–Thrower–Wales (STW) defect. The three defects studied in this work are predicted to have lower formation energies in silicene than in graphene. This could be beneficial in LIBs applications as defects play a crucial role in binding Li atoms. In all cases, Li is more strongly bound to silicene compared with graphene. The Li diffusion through hollow sites is mediated by a significantly lower energy barrier in silicene than graphene: 1.59 eV versus 8.38 eV for the pristine case, and 0.05 eV versus 1.72 eV for the DV. Unlike graphene, in silicene the barrier through the center of the SV is the highest. This is presumably due to the dangling bonds present. Using *ab initio*

calculations, Gao *et al* [61] investigated the structures, formation energies, migration behaviors and electronic/magnetic properties of typical point defects in silicene, including SW (also named STW) defect, SV, DV and adatom. The authors found that SW can be effectively recovered by thermal annealing. SV has much higher mobility than DVs and two SVs are very likely to coalesce into one DV to lower energy. Also, the existence of SW and DV may induce small gaps in silicene, while SV defects may transform semi-metallic silicene into metallic. Si adatoms as self-doping in silicene sheets can induce long-range spin polarization as well as a remarkable band gap, achieving all silicon magnetic semiconductors. Yang *et al* [62] performed first-principles calculations and studied the electronic structure and the quantum capacitance (QC) of silicene with defects and doping of N, P, B and S. They found that the QC of silicene was enhanced due to the appearance of localized states near the Fermi level. Moreover, they also studied the increase of the concentration of the doping and found that the QC improved. Moreover, Xu *et al* [63] studied with DFT calculations the effects of adsorption of Ti, Au, Ag, Cu and Al atoms with single vacancy defects and concentration variation. Again, they found that the doping enhanced the QC due to the presence of localized states in the proximities of the Fermi level. Momeni *et al* [58] investigated the QC of XSi_3 , being $X = P, Al, N, C, B$ and also studied these doped systems with defects. They found that the capacity of the doped systems improved, in comparison to pristine and defective silicene, mostly with the implementation of doping. The defects such as single vacancy (SV) and double vacancy (DV) did not significantly improve the QC of these systems. They attributed this enhancement to delocalized electronic states near the Fermi level, created mostly by 2p and 3p orbitals.

Despite the above, Li adsorption onto silicene is still not fully understood because of the lack of reliable experimental methods to make freestanding silicene so far. First-principle modeling is a powerful tool for battery research as it can accurately study the structural and electronic properties of electrode and electrolyte materials as well as the interactions between different materials.

The aim of the present work is to perform theoretical investigations for lithium atoms on silicene. We have analyzed the interaction of the different charge states in Li: Li atom (Li^0), Li-ion (Li^{+1}) and charged Li (Li^{-1}) with pristine and defected silicene single-layer and compare the performances among them. This is closer to the real battery behavior. We also analyzed the changes in the electronic structure and the charge density distribution through charge density difference diagrams in all cases. Charge density and the average open circuit voltages (OCV) are also reported. In addition quantum capacity (QC) calculations are addressed, for the first time, considering an adsorbed Li-ion on a substrate.

2. Methodology

2.1. Theoretical method

For the calculations of optimized geometrical structures and electronic properties of pristine and defective silicene

we use DFT with the projector augmented wave potentials method as implemented in the VASP code [64–66]. Valence electronic states and the core-valence interaction are described using periodic plane waves and Blöch's projector augmented wave (PAW) approach, respectively [67]. The exchange–correlation energy of interacting electrons was calculated using generalized gradient approximation with the Perdew–Burke–Ernzerhof (GGA-PBE) parameterization [68]. The valence electron configurations present are $1s^2 2s^1$, $[Ne] 3s^2 3p^2$ for Li and Si, respectively. To make sure that the total energy is converged at 1 meV/atom level, the appropriate plane-wave basis and k -space integral are chosen. For the plane wave expansion, the kinetic energy cutoff of 700 eV is determined to be enough. For the k -points grid, the Monkhorst–Pack method is used [69] with a $7 \times 7 \times 1$ k -point mesh. Methfessel–Paxton method is used for the partial occupancies for each orbital, with a smearing parameter of 0.05 eV. All the structures have been optimized until the forces acting in each atom are less than 0.02 eV/Å with a total energy change less than 1×10^{-4} eV. Stress tensors elements reached down to 1.0 kbar for the optimization of cell parameters. Spin polarized calculations were considered to take into account the possible magnetism of the defective systems. Based on lattice parameters of the primitive cell, we construct a supercell of 5×5 units with hexagonal structure. In order to prevent the artificial interaction of layers, a vacuum of 11 Å along the z direction is constructed. All structural models are fully relaxed. We considered three possible initial charge states ($q = +1, 0$ and -1) for the Li adsorption on the systems. The adsorption energy was calculated using the following equation:

$$E_{ad} = E_{system+Li^q} - E_{Li^q} - E_{system} \quad (1)$$

where, q represents the Li atoms charge, E_{Li^q} is the energy of a single charged Li atom, E_{system} is the pristine or defective silicene total energy and $E_{system+Li^q}$ is the total energy of the system after the adsorption. The defect formation energy was calculated according to:

$$E_{df} = E_{dsystem} - \frac{N-1}{N} E_{system} \quad (2)$$

where, E_{df} represents the formation energy of the system with the defect, $E_{dsystem}$ is the energy of the defective silicene, and N represents the number of Si atoms in the configuration. When both the volume and entropy effects are neglected, the open circuit voltage (OCV) can be obtained at each using the following equation [70]:

$$OCV \approx \frac{E_{Li^q} + E_{system} - E_{system+Li^q}}{e} \quad (3)$$

where e symbolizes the electronic charge.

It is well known that on an ideal metal the perfect screening can lead to the confinement of excess charge on the surface. This allows not considering the capacitance of a metal contact, which is usually a part of the electrode [71]. Silicene-based 2D materials do not have a good screening. Therefore, it is expected that their intrinsic capacitance (QC) has a prominent

influence on the performance of devices, such as supercapacitors and field-effect transistors, when these materials are used in electrodes [72, 73]. The QC can be defined by the formula:

$$C_Q = e^2 \int_{-\infty}^{+\infty} D(E) \frac{\sec h^2((E - e\Phi)/2k_B T)}{4k_B T} dE \quad (4)$$

where $D(E)$ is the density of states, Φ is the local potential, E is the relative energy with reference to the Fermi level, e is the elementary electric charge and k_B is the Boltzmann constant. In all calculations the T is set to room temperature (300 K) [74].

The doped systems were also studied with charge density difference plots. The calculations of the charge density difference were done with the following equation:

$$\rho = \rho_{\text{Total}}(r) + \rho_{\text{silicene}}(r) - \rho_{\text{Li}}(r) \quad (5)$$

where $\rho_{\text{Total}}(r)$, $\rho_{\text{Silicene}}(r)$ and $\rho_{\text{Li}}(r)$ are the total charge on the stable intercalation configuration, silicene and the Li atom, respectively.

2.2. Computational model

Silicene has a hexagonal crystalline system consisting of Si atoms in a $P\bar{3}m1$ space group. The atoms in this phase have three bonded neighbors. The unit cell consists of two Si atoms. The calculated lattice parameter, bond length and buckling height are $a = 3.87 \text{ \AA}$, Si–Si = 2.28 \AA , $\Delta z = 0.44 \text{ \AA}$, $\alpha = 90^\circ$, $\beta = 90^\circ$ and $\gamma = 60^\circ$, which are in good agreement with theoretical values reported [52, 54, 68]. Huang *et al* performed [59] DFT-GGA calculations and reported values of $a = 3.86 \text{ \AA}$, Si–Si = 2.27 \AA , $\Delta z = 0.45 \text{ \AA}$, which is in good agreement with our results.

After the optimization of this unit cell, a supercell of 5×5 surface of 50 atoms was constructed from the replication of the unit cell and afterward relaxed, which after relaxation consisted of lattice parameters with values of $a = 19.33 \text{ \AA}$, Si–Si = 2.28 \AA and $\Delta z = 0.44 \text{ \AA}$, $\alpha = 90^\circ$, $\beta = 90^\circ$ and $\gamma = 60^\circ$.

Then, Li atoms were adsorbed in this system, with a concentration of $x(\text{Li}) = 0.02$. At this concentration, no lattice strain is expected in the size of this supercell with vacuum. In all the calculations, the lateral displacement of the Li atom is restricted. The van der Waals calculation was tested for a hollow site in the pristine case for Li atom adsorption, finding an energy difference of 0.03 eV without considering the long-range interaction. Therefore, the van der Waals interactions were not included in the calculations.

3. Results and discussion

3.1. Geometry optimization and Li doping sites

Four different configurations of silicene were studied in this work, which are shown in figure 1. We have chosen high symmetry adsorption sites: top, bridge and hollow. All the same sites of the pristine structure were tested on the defect structures but, for simplicity, we only report the most stable ones. The selected defects are the most stable and studied for this

2D material [56]. The defect formation energy of all configurations was calculated according to equation (2), obtaining 3.40 eV, 3.73 eV and 2.09 eV for silicene with a SV, a DV and a STW defect, respectively. This tendency is in good agreement with that reported by Setiadi *et al* [56]. A higher formation energy is needed of broken bonds versus the reorientation of the bonds, which is consistent with obtaining a lower formation energy for the STW defect.

The possible adsorption sites in the different configurations of silicene are shown in figure 1. In this figure, the H denotes a six-fold hollow site in the perfect zone, H1 is a six-fold hollow site in the defect zone (DZ) and H2 represents a five-fold pentagonal hollow site in the defect zone. The top on a superior silicon atom, valley (top an inferior Si atom) and two-fold bridge sites in the perfect and defect zone are denoted by T, V, B, T1, V1 and B1, respectively. The defect sites are labeled SV, DV and STW, depending on the defective system. The adsorption for charged Li^q ($q = -1, 0, +1$) were tested. The results showed that in all cases the adsorption energy of positive charged Li was the biggest one. So, we only kept testing for the different possible sites stability for this charge. Also, this case is the most realistic situation after the simulations.

The calculated adsorption energies for most favorable sites, Li–Si bonds, height differences between silicene and Li atom (Δz) and OCV are summarized in table 1 for all doped configurations of the Li_xSi sheet. The adsorbed configurations are presented in figures S1–S4 in the supplementary material (SM) (<https://stacks.iop.org/JPCM/34/245001/mmedia>).

In the first place, the adsorption sites for the pristine case were studied. We tested Li on T, V, B and H sites. This last site was found to be the most stable one among the others by 0.24 eV in the neutral charge case, which is in good agreement with the results previously reported in the literature [56, 59]. It can be appreciated that the V site is the second most stable one. For all charged Li cases, the H site is the most stable one after adsorption, being the Li^{+1} the one with the highest stability.

In the following configurations, in the cases for Li^{-1} and Li^0 , the most stable sites obtained for Li^{+1} were also calculated for comparison.

In the SV configuration, nine different adsorption sites were tested, which are depicted in figure 1 for Li^{+1} . It was found that the SV site was the most stable by 0.02 eV in comparison with the hollow site near the vacancy (H1). The adsorbed Li^0 and Li^{-1} show the same tendency.

For Li^{+1} , in the DV configuration, eight different adsorption sites were tested, finding that the pentagonal site (H2) is the most stable one by 0.02 eV in comparison with the DV site. However, in the other two charged cases, the DV site was most stable.

A similar result was obtained in the STW configuration, in which the pentagonal site (H2) is more stable by 0.07 eV in comparison with the STW site for the adsorbed Li^{+1} . The same tendency is followed in the Li^0 and Li^{-1} cases.

The SV site at the SV configuration (see figure 1(b)) is overall the most stable one for the Li adsorption on the surface. This is in good agreement with the tendency reported by Setiadi *et al* [56]. Moreover, they find the tendency of energetic stability to be $\text{SV} > \text{DV} > \text{STW} > \text{H}$. In our case, we arrive at a

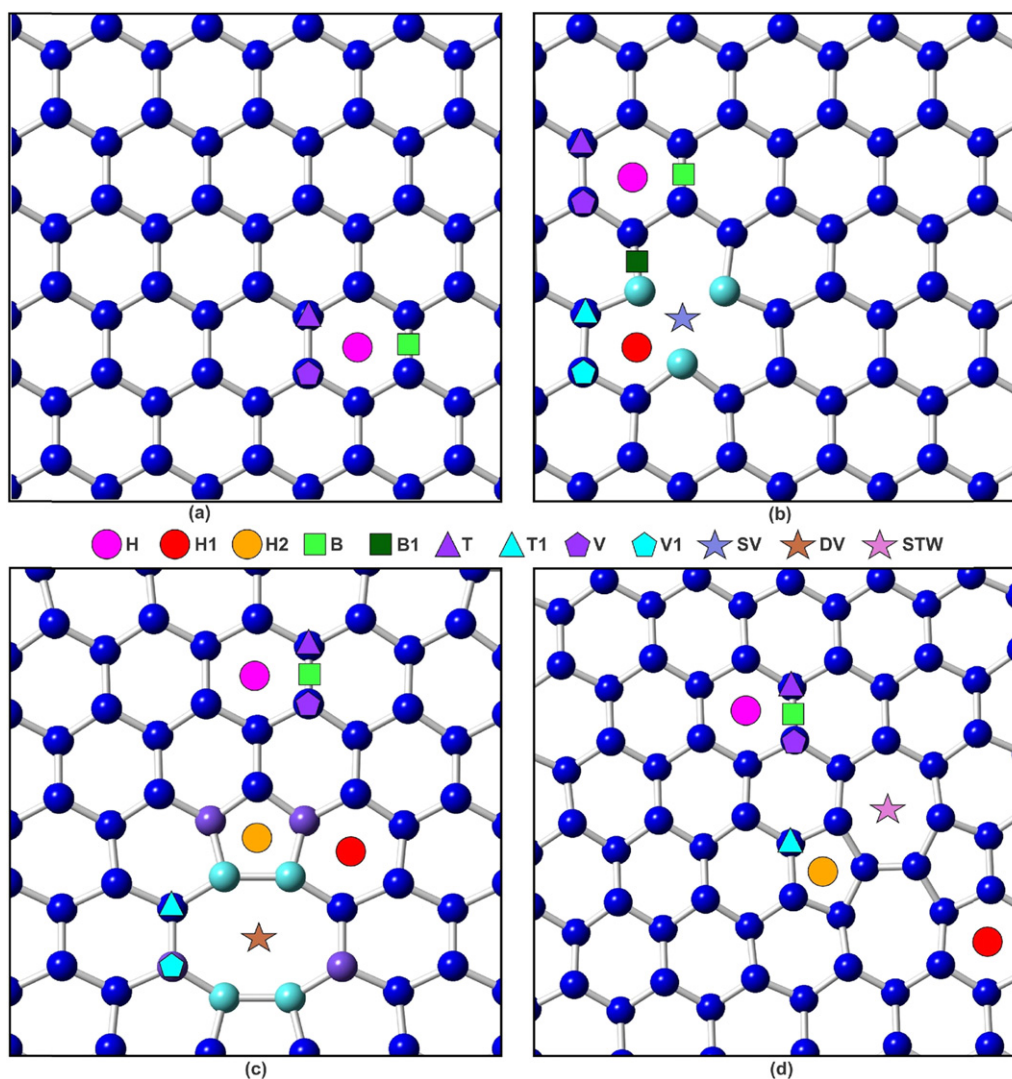


Figure 1. Schematic view of the pristine and defective silicene configurations with the possible adsorption sites: (a) pristine, (b) SV, (c) DV and (d) STW. The blue spheres represent Si atoms. The Si atoms that form the defective zones, DZ1 and DZ2, are indicated in cyan and violet spheres, respectively. H: six-fold hollow site, H1: six-fold hollow site close to the defected zone, H2: five-fold pentagonal hollow site close to the defected zone, B: bridge site, B1: bridge site close to the defect zone, T: top site, T1: top site close to the defected zone, V: valley site, V1: valley site close to the defected zone, SV: single vacancy defect site, DV: double vacancy defect site, STW: Stone–Thrower–Wales defect site.

different trend: SV (SV configuration) > H2 (STW configuration) > DV (DV configuration) > H (pristine configuration). The adsorption energy trend is related to the electrostatic interaction between the ion adsorbate and the defective substrate. This is in good agreement with the reported results by Pattara-pongdilok and Parasuk considering the same charged states of lithium on graphene quantum dots [75].

The diffusion of Li is an important point to be discussed on silicene. Nevertheless it deserves a separate analysis beyond the purpose of the actual work. Our preliminary NEB results show that the diffusion barriers for the SV, DV and STW defects are higher when compared with the pristine case, which is in good agreement with the adsorption energies and the tendency of the Li atom to stay in the defect. Moreover, we found that the Li^{+1} case has a slightly lower barrier in comparison with the Li^0 and Li^{-1} charged cases. Due to the rather scarce

studies of charged ions in silicene, it is appropriate to mention some results of charged ions in other monolayers. Yu *et al* has validated by DFT calculations that positive charged potassium ion has a smaller diffusion barrier than that of neutral potassium atom in transitional metal oxchalcogenides monolayers [76]. Furthermore, these barriers have low values in all the studied cases, which indicates that diffusion is not significantly affected by the implementation of defects. The calculated NEB barriers results are summarized in table S1 in the supplementary material.

Considering the geometry, in the pristine configuration (figure 1(a)), the longest bond corresponds to an H site for Li^{+1} , which is 0.19 Å longer than the shortest bond, which was the T site for Li^{+1} . Meanwhile, for the SV configuration, the longest bond corresponds to the H site for Li^{+1} far away from the defect zone, which is 0.22 Å longer than the shortest bond, which was the SV site for Li^{+1} . In the DV configuration,

Table 1. Adsorption energies (eV), Li–Si bond lengths (Å), height differences Δz (Å) and OCV (V) calculated values for Li^q adsorbed in pristine and defected silicene ($q = 0, -1, +1$). X indicates that these are not stable sites, the Li atom moves to a neighboring site. Moreover, — and * indicates that this site was not calculated and that the final position is below the upper buckled Si, respectively.

Structure/site	E_{ad} (eV)			Li–Si (Å)			Δz (Å)			OCV (V)		
	$q = -1$	$q = 0$	$q = +1$	$q = -1$	$q = 0$	$q = +1$	$q = -1$	$q = 0$	$q = +1$	$q = -1$	$q = 0$	$q = +1$
Pristine												
H	−1.20	−2.16	−4.29	2.67	2.69	2.72	1.34	1.38	1.47	1.20	2.16	4.29
T	−0.90	−1.72	−3.87	2.62	2.55	2.53	1.10	1.54	1.74	0.90	1.72	3.87
V	−0.98	−1.92	−4.07	2.62	2.60	2.61	1.65	1.74	1.80	0.98	1.92	4.07
B	X	X	−3.95	X	X	2.57	X	X	1.90	X	X	3.95
Defected—SV												
SV	−2.96	−3.31	−4.81	2.51	2.54	2.49	1.49	1.52	1.85	−2.96	3.31	4.81
H	—	—	−4.54	—	—	2.71	—	—	1.20	—	—	4.54
T	—	—	−4.40	—	—	2.56	—	—	1.80	—	—	4.40
V	—	—	−4.51	—	—	2.61	—	—	1.77	—	—	4.51
B	—	—	−4.28	—	—	2.60	—	—	1.83	—	—	4.28
H1	−2.82	−3.22	−4.79	2.62	2.65	2.68	1.58	1.61	1.67	−2.82	3.22	4.79
T1	—	—	−4.20	—	—	2.54	—	—	1.69	—	—	4.20
V1	—	—	−4.34	—	—	2.60	—	—	1.63	—	—	4.34
B1	—	—	−4.45	—	—	2.69	—	—	1.70	—	—	4.45
Defected—DV												
DV	−2.67	−2.88	−4.30	2.69	2.69	2.68	0.13*, 0.18	0.18*, 0.13	0.01	2.67	2.88	4.30
H	—	—	−4.19	—	—	2.72	—	—	1.40	—	—	4.19
T	—	—	−3.81	—	—	2.55	—	—	1.71	—	—	3.81
V	—	—	−3.93	—	—	2.62	—	—	1.86	—	—	3.93
B	—	—	−3.86	—	—	2.60	—	—	1.85	—	—	3.86
H1	—	—	−4.29	—	—	2.75	—	—	1.42	—	—	4.29
T1	—	—	−4.06	—	—	2.61	—	—	1.66	—	—	4.06
V1	—	—	−3.95	—	—	2.61	—	—	1.82	—	—	3.95
H2	−2.10	−2.58	−4.32	2.66	2.68	2.68	1.66	1.68	1.72	2.10	2.58	4.32
Defected—STW												
STW	−1.83	−2.46	−4.41	2.60	2.61	2.71	1.07	1.19	1.07	1.83	2.46	4.41
H	—	—	−4.29	—	—	2.73	—	—	1.38	—	—	4.29
T	—	—	−3.90	—	—	2.54	—	—	1.57	—	—	3.90
V	—	—	−4.06	—	—	2.62	—	—	1.78	—	—	4.06
B	—	—	−3.98	—	—	2.59	—	—	1.72	—	—	3.98
H1	—	—	−4.35	—	—	2.69	—	—	1.37	—	—	4.35
T1	—	—	−4.41	—	—	2.67	—	—	1.20	—	—	4.41
H2	−1.88	−2.47	−4.48	2.61	2.63	2.69	1.31	1.17	0.96	1.88	2.47	4.48

the longest bond corresponds to the H1 site for Li^{+1} , which is 0.20 Å longer than the shortest bond, which was the T site for Li^{+1} . For the STW configuration, the longest bond corresponds to the STW site for Li^{+1} , which is 0.25 Å longer than the shortest bond, which was the T site for Li^{+1} site. The reported bonds are shown in magenta on figures S1–S4.

The bond distance results for the different configurations show that the shortest one overall is in the case of the Li^{+1} doping in the SV site of the SV configuration. Setiadi *et al* [56] obtained values of 2.31 Å for the SV site in the SV configuration and 2.78 Å for the H site in the pristine configuration, which are in good agreement with our results of 2.49 Å and 2.72 Å, respectively. Osborn *et al* [55] obtained a 2.64 Å bond average Li–Si length for a concentration of Li of $x =$

0.5, which is in good agreement with our results, in which we obtained a bond average of 2.63 Å. Moreover, it can be seen that the T site has one of the shortest distances in most of the configurations.

The calculated values for the height differences show that the highest one is the B site for the pristine configuration. Moreover, it can be appreciated that the height differences are higher for the Li^{+1} case in the pristine and SV configurations. In the DV configuration, the lowest heights are for the Li^0 and Li^{-1} cases, in which the lithium atoms are located below the upper Si atom by 0.18 Å and 0.13 Å, respectively, which is in good agreement with that reported by Setiadi *et al* [56]. In the DV case, the open space available in the substrate because of

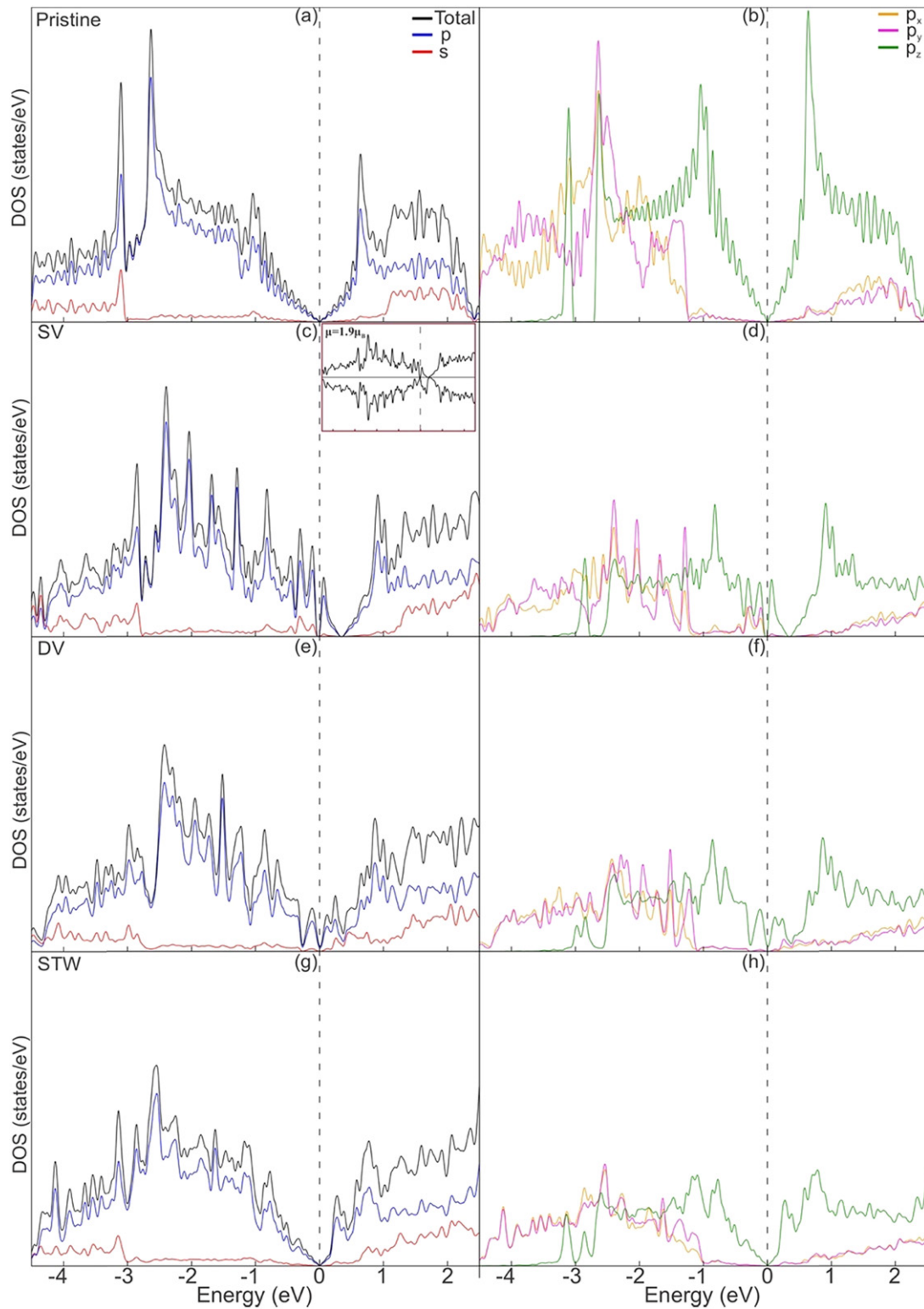


Figure 2. Total and Si atom orbital projected DOS curves for pristine silicene: (a) and (b); SV configuration (c) and (d); DV configuration (e) and (f) and STW configuration (g) and (h). The dashed line at zero corresponds to the Fermi level. The insert in figure (c) is the spin polarized DOS curves around the Fermi level for the silicene with a vacancy.

the absence of two Si atoms contributes to the low height for the adsorbed Li.

In all considered cases, the OCV in $\text{Li}^{+1}(\text{Li}^{-1})$ -doped systems are higher (lower) than pristine silicene. The average OCV for pristine silicene are 1.03 V, 1.93 V and 4.04 V for

$q = -1$, $q = 0$ and $q = +1$ respectively. For the defected silicene, the average OCV for the three charges follow the trend $\text{SV} > \text{DV} > \text{STW} (> \text{pristine})$, except for $q = +1$ in the DV system that has a lower value than the STW one. The OCV for $q = +1$ is the highest in all systems, suggesting that doping

silicene with Li^{+1} could be a suitable strategy for Li dispersing in LIBs electrodes. The obtained OCV values for defected silicene are higher than the corresponding values for N-doped [77] graphene and graphenylene [78], which makes silicene an excellent material for enhancing battery performance.

Considering that Li^{-1} ion adsorptions are the less stables for all systems, we only take into account the Li^0 and Li^{+1} most stable adsorbed configurations for the further analysis.

3.2. Electronic structure, charge density difference and Bader analysis

3.2.1. Electronic structure. Regarding the electronic structure, figure 2 shows the total and projected DOS curves for pristine and defective systems. Almost all systems present a symmetric spin up and spin down contributions to the DOS, only the case of silicene with an SV is asymmetric with a magnetic moment of $1.85 \mu_B$ (see figure 2 and insert in figure 2(c)). These results are in good agreement with those reported by Ali *et al* [79]. It can be seen from figure 2(a) that the total DOS for the pristine silicene shows a semiconductor behavior, with intersecting conduction and valence bands at the Fermi level (E_F). The PDOS shows that the states at the valence band (VB) edge arise mainly from the p_z orbitals of the Si atom, while the conduction band (CB) edge is composed by the hybridization of the s and p_z orbitals. Also, the states between -4 eV and -2 eV are formed mainly by a strong hybridization of orbitals s, p_x and p_y (see figure 2(b)). The vacancy defects are localized states; they give rise to localized states around the Fermi level. These states move the E_F down into the VB and give a metallic character to SV and DV defective silicene (see figures 2(c) and (e)). The vacancy defects act on electronic properties of silicene in a similar way as by p-doping, which shifts down the Fermi level into the VB. The overlap of the p_z orbitals is altered in the vicinity of the structural defects, leading to a local rehybridization of the s, p_x and p_y orbitals which is responsible of the changes on the electronic structure of vacancy defective systems (see figures 2(d) and (f)). Also, it is important to note that the DV case presents the stronger hybridization. These results are in good agreement with those reported by Hernandez Cocolletzi and Castellanos Águila and Momeni *et al* [58, 80].

In the case of silicene with the STW defect, no pronounced changes in the DOS plot can be observed when it is compared with the pristine case (compare figures 2(a), (b) and (g), (h)).

The total and projected DOS curves after neutral and positive charged Li atom adsorption on the most stable sites for pristine and defective systems are presented in figures 3 and 4. Only the spin up contribution is plotted, because all systems have symmetric spin up and spin down contribution after adsorption. It can be seen in figure 3(a) that when the Li^0 is adsorbed at an H site on pristine system, the Dirac cone has a right shift relative to the Fermi level, which is consistent with an n-type doping character. The $s-p_z$ orbital hybridization of Li–Si interaction is responsible for this. The edge VB and CB states are mainly composed by the Si p_z orbital, but between -4 eV and -2 eV the states are mostly formed for a hybridization of s, p_x and p_y orbitals of Si and s orbital of

Li (see figures 3(b) and (c)). These results agree with that reported by Hussain *et al* [81]. In the case of Li adsorbed at the SV and H1 sites on the SV system, the Fermi level is shifted to the VB showing a p-type doping character (see figures 3(d) and (g)). The Li–Si bond is formed by a hybridization of $s-p_z$ orbitals near the E_F (figures 3(e), (f), (h) and (i)). In the case of the DV system, for both adsorption sites, the DOS curves show a metallic behavior (see figures 3(j) and (m)). The states on the Fermi level are composed by a strong hybridization of Li s and Si p_z orbitals. For the Li atom adsorbed at the STW site of STW configurations, figures 3(p) and (q) show a metallic behavior due to a strong hybridization of $s-p$ orbitals of Li–Si interaction. At the H2 site on this system, the most important changes are in the end of VB due to Li s orbitals and Si p_z orbitals hybridization between -0.5 eV and the E_F (see figures 3(s)–(u)). All these results are consistent with a charge transfer from Li to silicene pristine and defective systems.

In the case of Li^{+1} adsorption at the H site of pristine silicene, figure 4(a) shows a similar behavior in comparison with the undoped case. The interaction between Li and Si appears in the beginning and in the end of valence and conduction band, respectively. In the beginning of the VB, the states are formed mostly by a hybridization of s, p_x , p_y orbitals of Si and s orbital of Li, while the end of CB is composed by Li s orbitals and Si s and p orbitals (see figures 4(b) and (c)).

For the Li^{+1} adsorbed at the most stables sites on the SV system and at the DV site of the DV configuration, the DOS curves behavior is similar to that of Li^0 adsorption but with a different shift, which is consistent with a different amount of charge transfer in both cases (see figures 4(d)–(l)). In the positive charged Li adsorbed at the H2 site, the E_F is shifted to the end of the VB due to the $s-p_z$ orbitals hybridization of Li and Si atoms near the Fermi level (see figures 4(m)–(o)). In the STW system, when the Li^{+1} is adsorbed at the STW site, the DOS curves do not present important changes near the Fermi level, were the dominant state are the Si p_z orbitals (see figures 4(p)–(r)). Finally, for the H2 site on the STW configuration, figures 4(s)–(u) show that the E_F is at the beginning of the CB due to the interaction of the s and p_z orbitals of Li and Si atoms around the Fermi level.

3.2.2. Charge density difference. The charge density difference plots for the adsorption of Li^0 , Li^{+1} at the most stable sites of the pristine and defective systems are shown in figure 5.

It can be seen that for Li^0 adsorption cases, the charge transfer is located in the vicinity of the Li atom adsorption site. For all configurations of the Li^{+1} ion adsorption, an intermediate situation occurs, a charge transfer from the surface to the Li atom vicinity is present. Moreover, in all plots, it can be appreciated that the charge density distribution depends on the adsorption position of the Li atom and atoms distribution in the configuration in which it is adsorbed (see figure 5).

We have performed Bader charge analysis [82] at the most stable adsorption sites of neutral and positive charged Li on the system of study. All of these systems and adsorption configurations show that Li^0 atom has a final charge about of $+0.9e^-$, indicating a charge transfer to the silicene surface. This is consistent with a cationic behavior of Li atom and

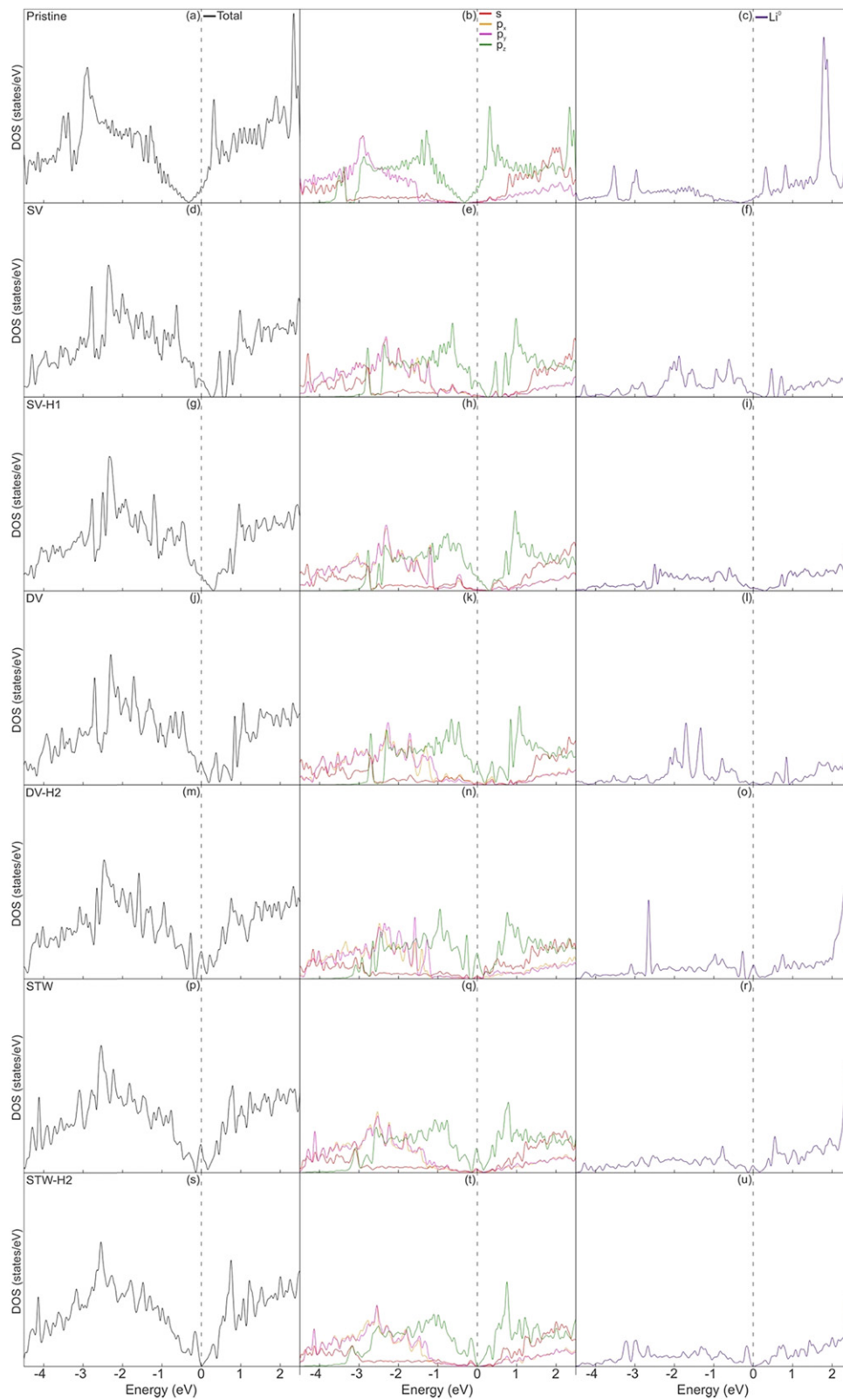


Figure 3. Total and Si atom orbital projected DOS curves for Li^0 atom adsorbed at: H site on pristine silicene (a)–(c); SV site on SV configuration (d)–(f); H1 site on SV configuration (g)–(i); DV site on DV configuration (j)–(l); H2 site on DV configuration (m)–(o); STW site on STW configuration (p)–(r) and H2 site on STW configuration (s)–(u). The dashed line at zero corresponds to the Fermi level.

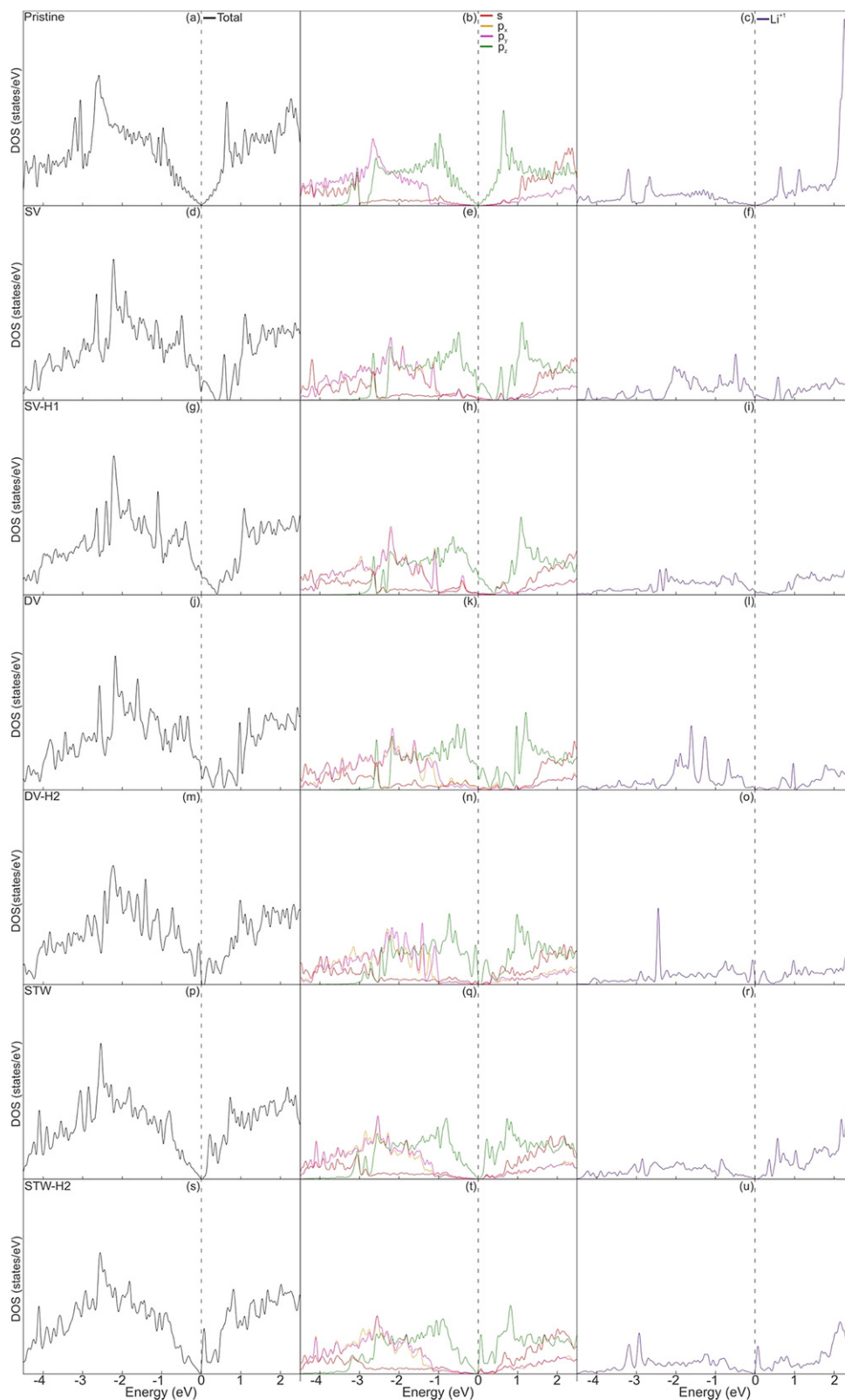


Figure 4. Total and Si atom orbital projected DOS curves for Li^{+1} atom adsorbed at: H site on pristine silicene (a)–(c); SV site on SV configuration (d)–(f); H1 site on SV configuration (g)–(i); DV site on DV configuration (j)–(l); H2 site on DV configuration (m)–(o); STW site on STW configuration (p)–(r) and H2 site on STW configuration (s)–(u). The dashed line at zero corresponds to the Fermi level.

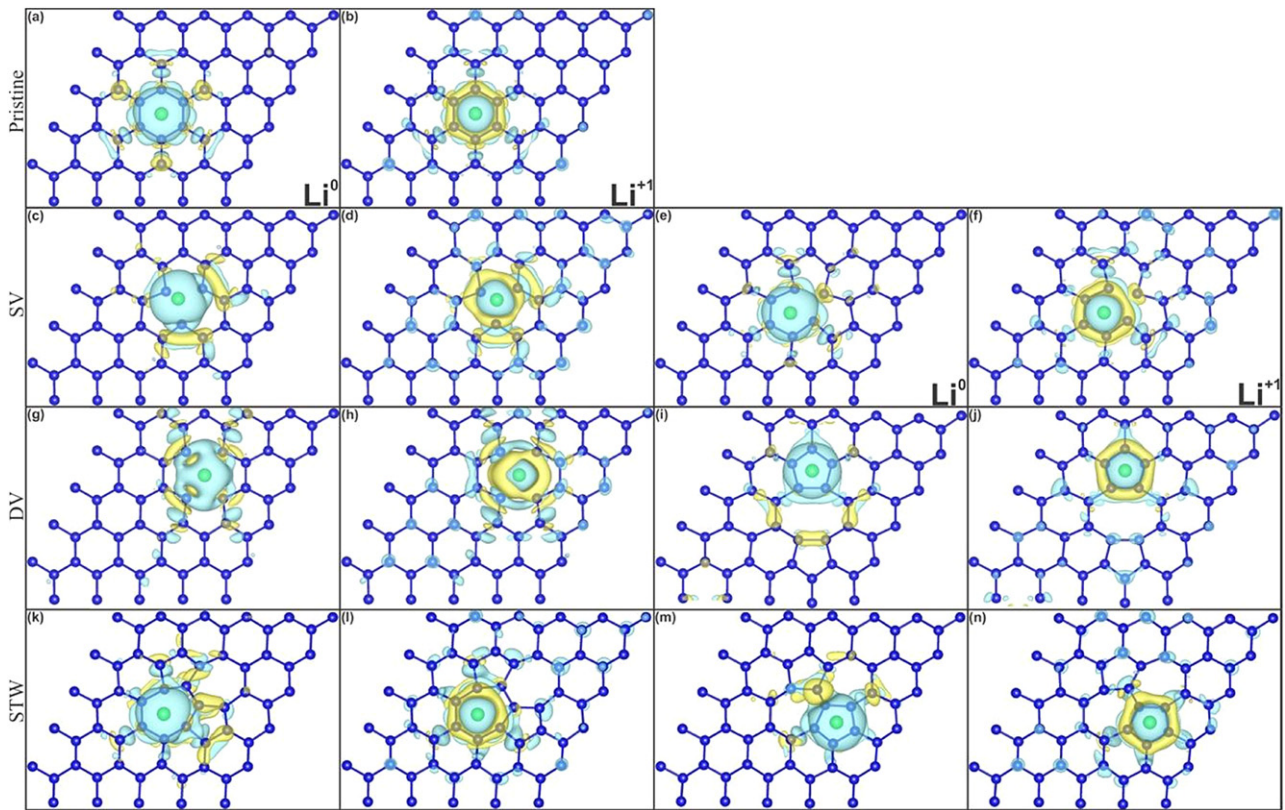


Figure 5. Isosurface plots at $0.0003 \text{ e}/\text{\AA}^3$ for Li^0 atom intercalated at the most stable sites of pristine and defective systems ((a), (c), (e), (g), (i), (k), (m)); Li^{+1} ion intercalated at the most stable sites of pristine and defective systems ((b), (d), (f), (h), (j), (l), (n)). The light blue area represents electron loss, while the yellow area represents electron gain. The blue and green spheres represent Si and Li species, respectively.

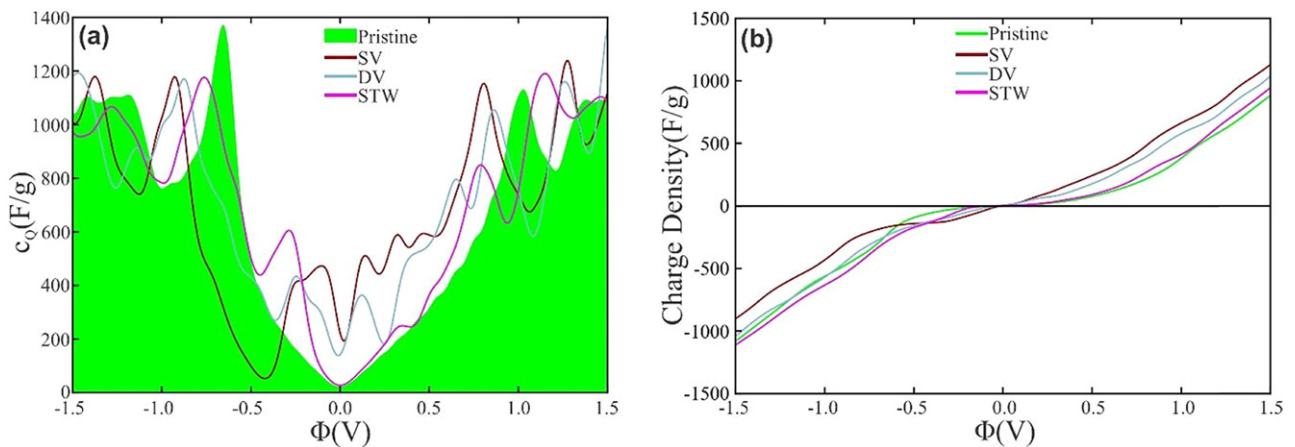


Figure 6. Quantum capacity vs local electrode potential (a) and charge density vs local electrode potential (b) for the pristine and defective system.

anionic character of the surface. The charge transfer occurs due to the sp hybridization of the Li-Si bond. For Li^{+1} adsorption, the charge change from $+1$ to about $+0.9e^-$, which implies some charge transfer to the surface. This behavior is similar to that reported for Li^+ ion adsorbed on pristine and defective graphene sheets [83, 84]. The results are in good agreement with the results shown in the charge density differences plots and DOS curves.

3.2.3. Quantum capacity analysis. The calculated QC and charge densities vs local electrode potential of the pristine

and the defective configurations are shown in figure 6. The green area in figure 6(a) represents the QC for the pristine case, with a maximum shown at approximately -0.6 V . Also, it presents the lowest curve in the positive charge zone (see green curve in figure 6(b)), which is consistent with the few states below the proximities of the E_F on the PDOS curves shown in figure S5(a) in the SM. These results are in good agreement with those reported by Momeni *et al*, Xu *et al* and Yang *et al* [58, 62, 63].

In the case of the SV configuration, the dark red curve in figure 6(a) shows that the Dirac point is moved to the left,

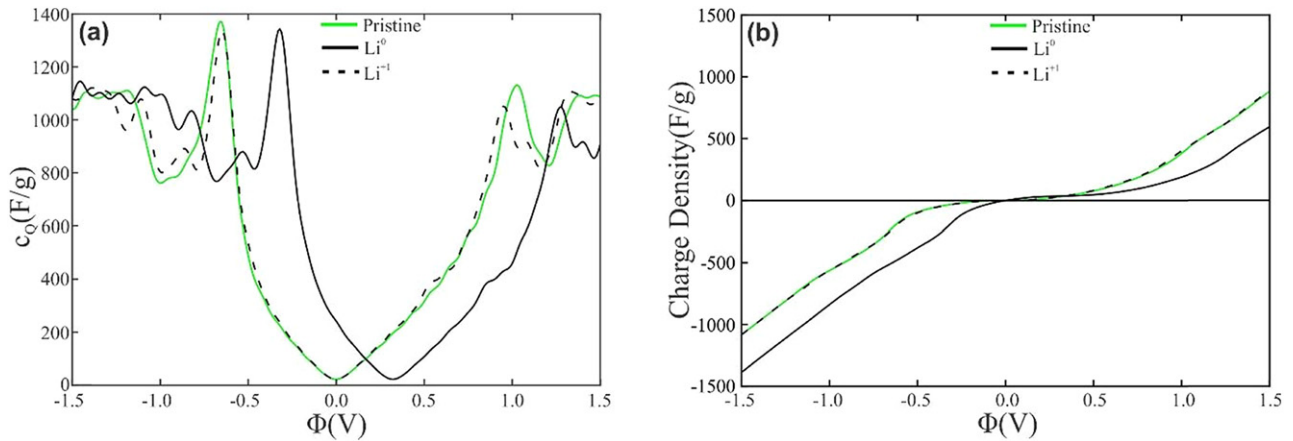


Figure 7. Quantum capacity vs local electrode potential and charge density vs local electrode potential for pristine silicene with and without Li adsorption at the H site.

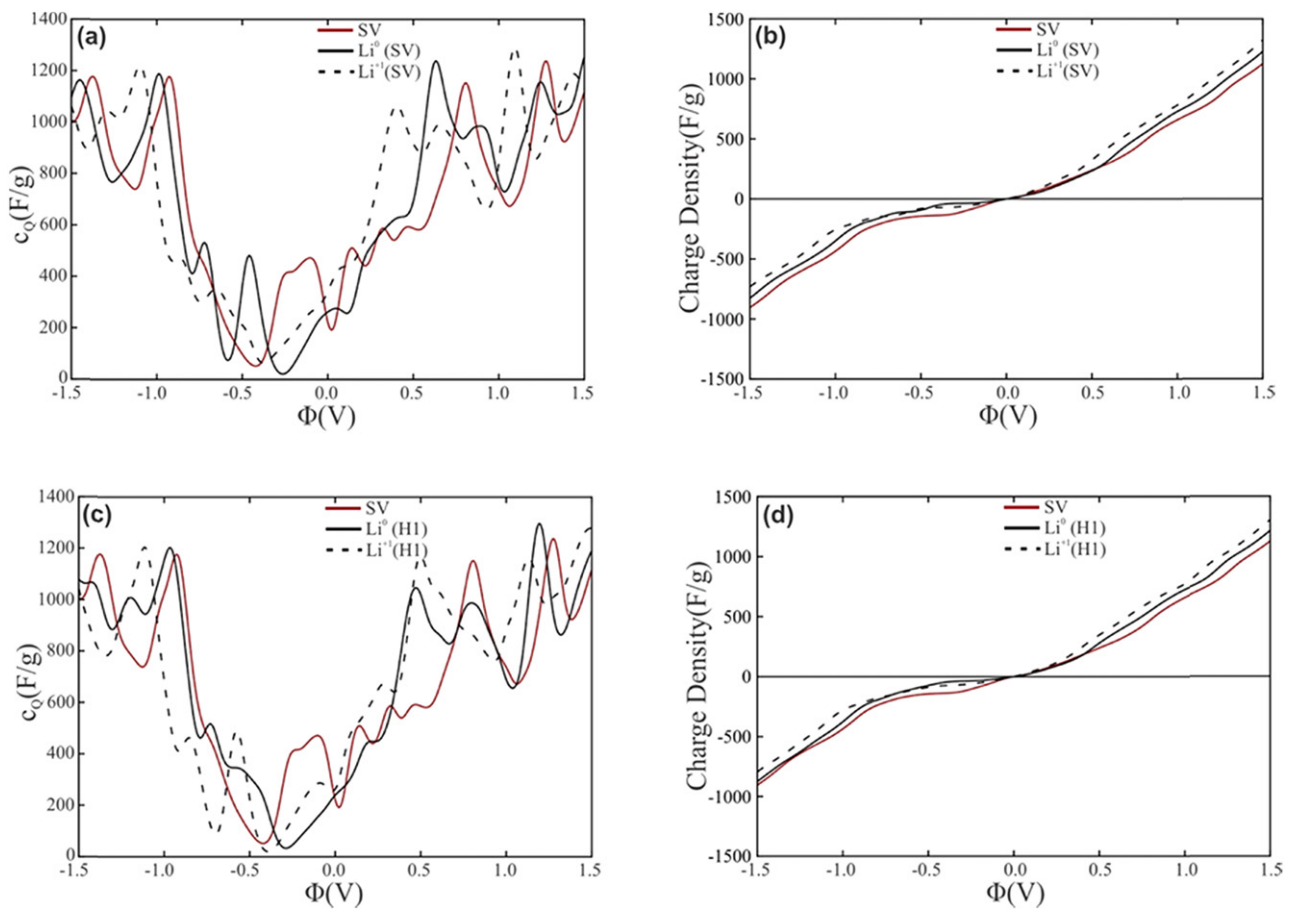


Figure 8. Quantum capacity vs local electrode potential and charge density vs local electrode potential for SV silicene with and without Li adsorption at the SV site ((a) and (b)); and at H1 site ((c) and (d)).

near -0.5 V, while for the charge density vs Φ plot, it shows in figure 6(b) a predominance in the positive charge zone and that it is the less predominant in the negative zone. This behavior is a consequence of an important number of states induced by the defect around the E_F (see figure S5(b) in SM). Moreover, this produces the SV configuration have an improved QC in comparison to the pristine case, which can be seen in the positive voltages. For the DV configuration curve in light blue

in figure 6(a), the minimum of the QC vs Φ remains at approximately 0 V. The charge density vs Φ curve in this case is the second most predominant in the positive zone (see figure 6(b)). This is due to the presence of defect states below the proximities of the E_F in the PDOS curves in figure S5(c) in SM. Also, it produces the secondary best improvement of QC just below the SV system, as it can be seen in figure 6(a). It is important to note that the atoms at DZ1 produce more states around the

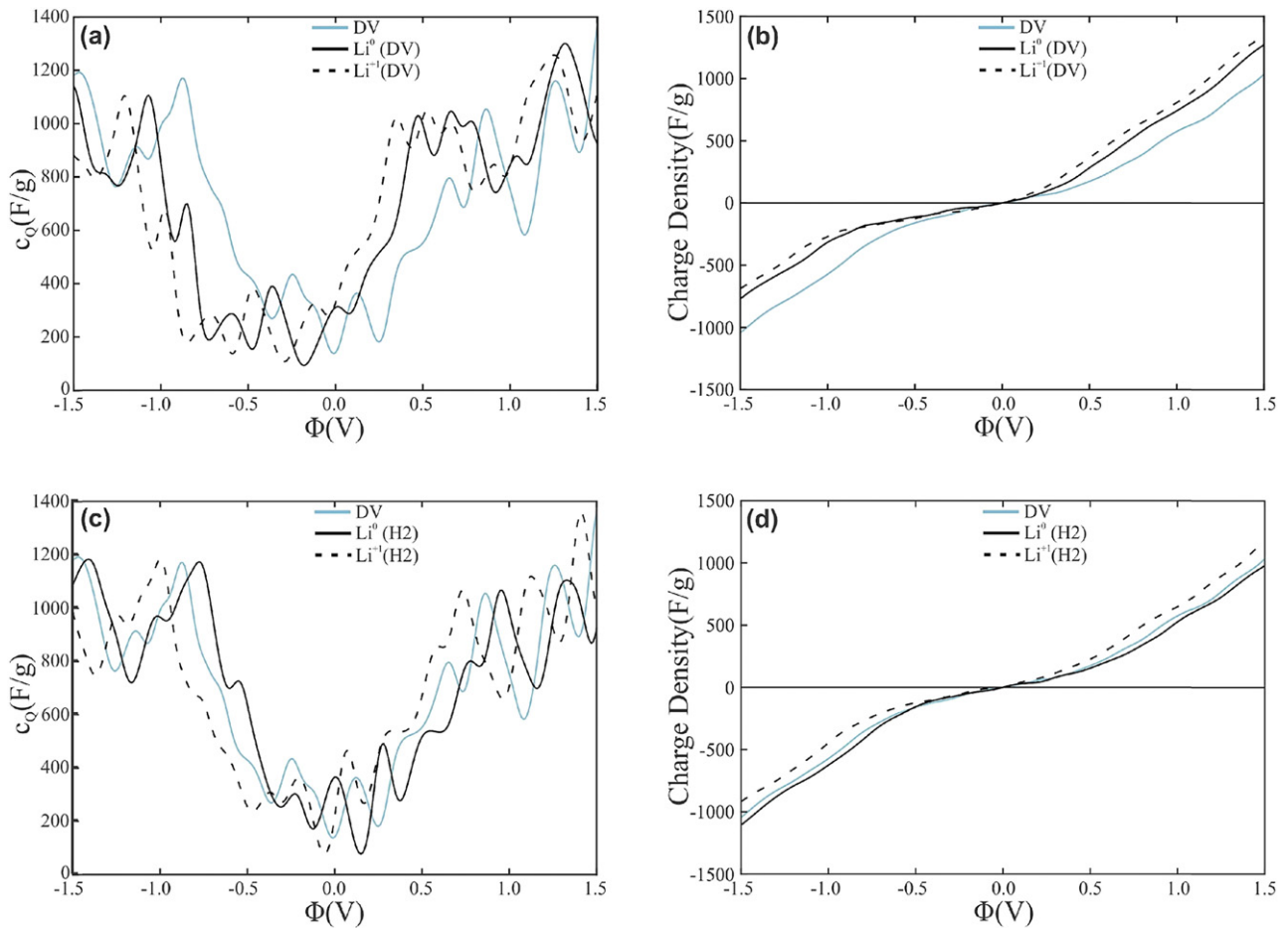


Figure 9. Quantum capacity vs local electrode potential and charge density vs local electrode potential for DV silicene with and without Li adsorption at the DV site (a) and (b)); and at the H2 site (c) and (d).

Fermi level than those at the DZ2 (see figure S5(c)). These agree with those reported by Yang *et al* [62].

The dark pink curve in the QC vs Φ in figure 6(a) corresponds to the STW configuration and in general remains very similar to the pristine case, which is in good agreement to the results obtained by Momeni *et al* [58]. The STW configuration is the predominant one in the negative zone for the charge density vs Φ plot in figure 6(b). The PDOS in figure S5(d) in SI shows similarity with the pristine case, which is consistent with the similarities in QC.

These results show that generating defects produces an improvement on charge density in the positive voltage zone and an enhancement of QC of silicene in positive bias due to the 3p orbitals of Si atoms in defective zones, which is necessary for better supercapacitors.

Figures 7–10 show the plots of the QC, charge density for pristine and defective systems doped with neutral and positive charged lithium atom in the most stable configurations.

The quantum capacity plot for the doped pristine configuration is shown in figure 7(a). It can be appreciated for the Li^0 adsorbed at the H site, a displacement of the quantum capacity to positive values (which is consistent with the shifts of the E_F seen in the PDOS in figure S6(a) in SM) and also an enhancement of QC in negative biases. The doping with Li^{+1}

ion does not produce an increase in the QC and is similar to the pristine case, which agrees well with the comparison of the PDOS of the pristine case before and after adsorption of Li^{+1} at the H site (figures S5(a) and S6(b)). Therefore, the charge density curves in figure 7(b) show a perfect match between the pristine and the Li^{+1} cases, while for the Li^0 doped system a predominance in the negative charge density zone is shown.

In the case of the doped SV configurations, in figures 8(a) and (c), it can be seen that the adsorption of neutral and positive charged lithium at the most stable sites produces an increase in the maximum of the quantum capacitance. This is consistent with more positive PDOS states below E_F in figure S7 in SM, which translates in an increase of the positive QC. Moreover, the displacement of the graphs of the doped Li system in comparison with the SV silicene is in the same trend as in figure 7(a), the Li^{+1} adsorbed configurations has its minimum near the SV case, while the Li^0 configurations are displaced to the right. Accordingly, the charge density in figures 8(b) and (d) shows that the Li^{+1} systems have the most positive charge density.

Comparing the DV system before and after adsorption of neutral and positive charged lithium produces an increase in QC in positive voltage values (compare figures 9(a) and (c) with figure 6(a)). This increase can be related with PDOS

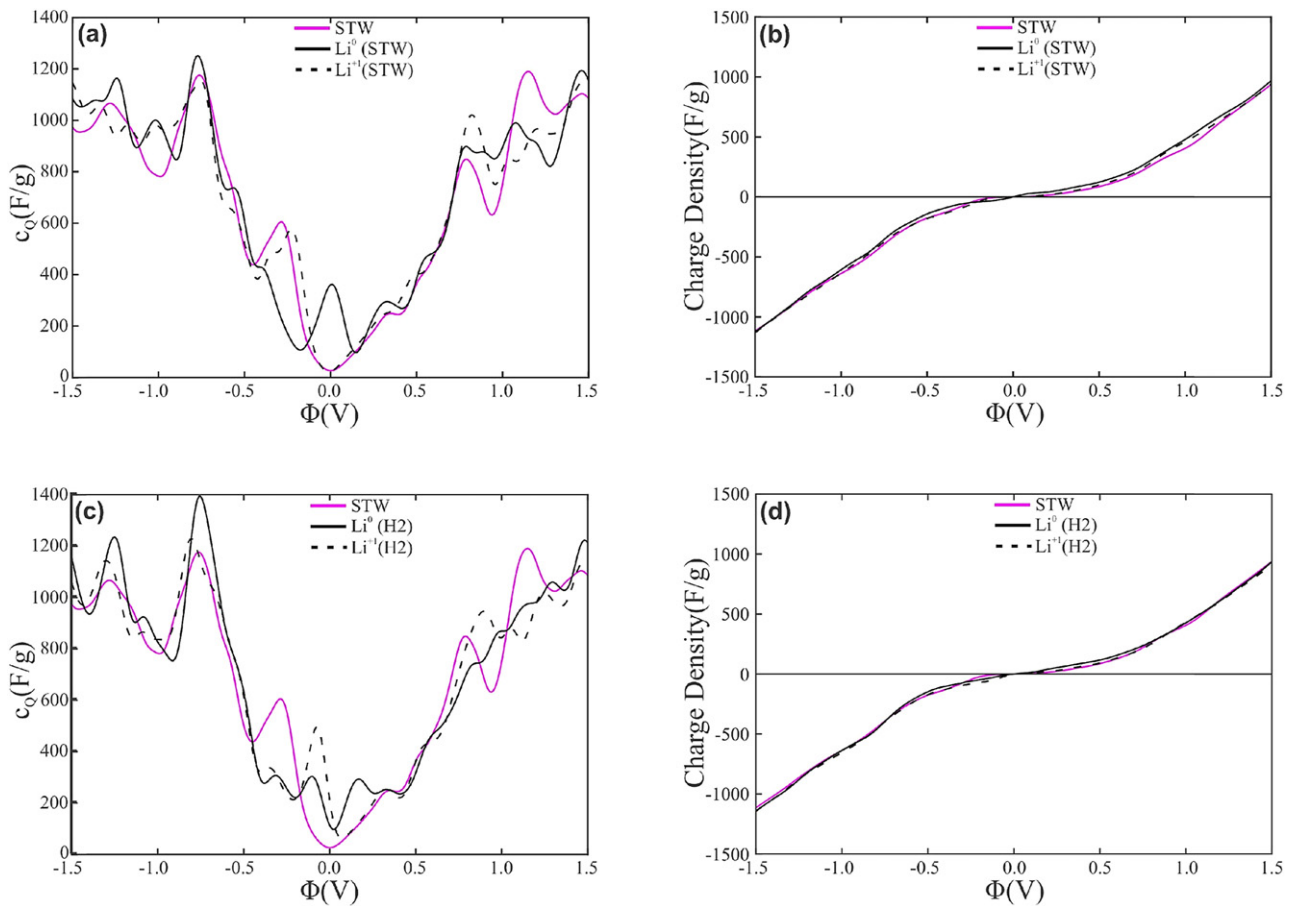


Figure 10. Quantum capacity vs local electrode potential and charge density vs local electrode potential for SV silicene with and without Li adsorption at the STW site ((a) and (b)); and at the H2 site ((c) and (d)).

showing more states below the E_F (see figure S8 in SM). Moreover, the displacement of the graphs for doped Li DV systems is different in comparison with the pristine and the SV cases. Here, the Li^0 and Li^{+1} curves are displaced to negative values. The charge density in figures 9(b) and (d) show that the DV system has the most negative charge density, whereas the Li^{+1} and Li^0 systems have the higher charge density in positive voltages in comparison with the DV undoped case, which agrees with the results obtained before.

For Li^0 and Li^{+1} adsorbed at the DV site, it can be seen that minimum is shifted to negative values, while in the case of Li^+ adsorbed at the H2 site, the minimum is again almost at 0 V and for Li^0 is moved to positive values (see figures 9(a) and (c)). Again, we see an increase in the QC for the different cases. In the positive voltages, the Li^{+1} curve shows an enhancement, in contrast to the Li^0 case. Meanwhile, in the negative voltages, the Li^0 curve shows an enhancement. The charge densities in figures 9(b) and (d) show that the Li^{+1} case is the most positive one. These results are consistent with the behavior of the PDOS around the Fermi level for the different DV configurations (see figure S8 in SM).

For Li adsorbed at the STW site of the STW system in figure 10(a), the QC shows an enhancement in the Li^0 case in the positive voltages. However, this enhancement is not as relevant as the defective cases previously described. The PDOS

of the Li^0 case shows more presence of states below the E_F (see figure S9(a) in SM). The lithium curves show positive displacement for Li^0 , while the Li^{+1} curve shows no displacement. For the charge densities in figure 10(b), the Li^0 curve is the most positive one. For these curves, we see that they are almost all superimposed.

Finally, in the case of Li adsorbed at the H2 site on the STW system, figure 10(c) shows a general shape similar to figure 10(a). The doped curves show a closer minimum to 0 V and the maximum of Li^0 is higher at the H2 site than at the STW site. For this case only, there is no noticeable enhancement and displacement of the curves produced by the doping of Li. The PDOS do not show great differences between the doped cases (see figure S9 in SM). The charge densities presented in figure 10(d) show that they are all almost superimposed, but it can be barely noticeable that the Li^0 is the most positive curve.

In general, we see that the doping produces enhancements in the quantum capacities and charge densities and therefore making these facts useful to analyze these systems for future application. Moreover, for the case of SV and DV doped sites, a significant increase in the positive voltages in the QC is shown, mostly for the Li^{+1} case. These changes are due to 3p orbitals of Si atoms in defective zones. The case of the STW doped system in the H2 site is the one with small enhancement in

QC. In addition, the lithium doping shows to have an effect in the displacement of the curves, due to the different charge values considered.

4. Conclusions

Li^q ($q = -1, 0$ or $+1$) doping, in a low concentration, on different sites of pristine and defective silicene was theoretically studied. The comparative highest stability and OCV were found at the H site for the pristine case, at the SV site for the SV system and at the H2 site for the DV and the STW configurations. The highest adsorption energies were found to be for the Li^{+1} doped systems. The DOS curves are symmetric in all cases, except for the SV system that presents a magnetic moment of $1.85 \mu_B$. Furthermore, defect introduction generates states around the Fermi level, acting as a p doped system in the electronic structure, which is more visible at the SV site. The DOS curves for the pristine systems after Li adsorption show a shift of the Fermi level toward the CB, while in the case of the SV configurations is shifted to the VB. In the DV case, for Li^0 and Li^{+1} , there is a shift toward the CB and VB, respectively. The charge density difference and Bader analysis of the lithiated systems show that there is a local charge transference from Li to the surface. The charge transfer for Li^{+1} is more distributed on the silicene surface than for the Li^0 adsorbed systems. The QC and charge density analysis of the four configurations with and without doping show a good agreement with the DOS curves. From the pristine and the defective configurations comparison, it was found that the addition of defects in the systems generate an improvement in the positive voltages of the charge density and QC curves, due to the presence of 3p orbitals of Si atoms in the defective areas. In the doped systems the QC and charge densities in general showed an enhancement, mainly because of the hybridization of s-p orbitals of the Li-Si bond. There is an increase in the QC in positive bias for the SV and DV doping sites, predominant in the Li^{+1} cases, while this behavior is not present in the STW configurations. These QC and charge density improvements are useful for application in battery anodes.

Acknowledgments

Our work was supported by ANPCyT through PICT 2019-03491 Res. No. 015/2021, PICT 2017-2358, PIP GI-CONICET 2021-2023 code: 11220200100944CO and PIP GI-CONICET 2021-2023 code: 11220200100941CO research grants, as well as by SGCyT-UNS. EAG, PVJ and PB are members of IFISUR-CONICET. JJ, JV and FG are fellow researchers at this institution. RF and LF-W acknowledges PEDECIBA, CSIC-UdelaR and ANII, all Uruguayan Institutions for financial support.

Data availability statement

No new data were created or analysed in this study.

ORCID iDs

Julián Juan  <https://orcid.org/0000-0001-6408-060X>
 Paula V Jasen  <https://orcid.org/0000-0002-8088-8438>
 Ricardo Faccio  <https://orcid.org/0000-0003-1650-7677>
 Estela A González  <https://orcid.org/0000-0001-8128-6837>

References

- [1] Ashraf N, Isa Khan M, Majid A, Rafique M and Bilal Tahir M 2020 A review of the interfacial properties of 2D materials for energy storage and sensor applications *Chin. J. Phys.* **66** 246–57
- [2] Luo W, Ma Y, Gong X and Xiang H 2014 Prediction of silicon-based layered structures for optoelectronic applications *J. Am. Chem. Soc.* **136** 15992–7
- [3] Yu Y X 2019 Effect of defects and solvents on silicene cathode of nonaqueous lithium–oxygen batteries: a theoretical investigation *J. Phys. Chem. C* **123** 205–13
- [4] Chowdhury S and Jana D 2016 A theoretical review on electronic, magnetic and optical properties of silicene *Rep. Prog. Phys.* **79** 126501
- [5] Takeda K and Shiraishi K 1994 Theoretical possibility of stage corrugation in Si and Ge analogs of graphite *Phys. Rev. B* **50** 14916–22
- [6] Guzmán-Verri G G and Lew Yan Voon L C 2007 Electronic structure of silicon-based nanostructures *Phys. Rev. B* **76** 075131
- [7] Lin C-L, Arafune R, Kawahara K, Tsukahara N, Minamitani E, Kim Y, Takagi N and Kawai M 2012 Structure of silicene grown on Ag (111) *Appl. Phys. Express* **5** 045802
- [8] Feng B, Ding Z, Meng S, Yao Y, He X, Cheng P, Chen L and Wu K 2012 Evidence of silicene in honeycomb structures of silicon on Ag (111) *Nano Lett.* **12** 3507–11
- [9] Vogt P, De Padova P, Quaresima C, Avila J, Frantzeskakis E, Asensio M C, Resta A, Ealet B and Le Lay G 2012 Silicene: compelling experimental evidence for graphene like two-dimensional silicon *Phys. Rev. Lett.* **108** 155501
- [10] Fleurence A, Friedlein R, Ozaki T, Kawai H, Wang Y and Yamada-Takamura Y 2012 Experimental evidence for epitaxial silicene on diboride thin films *Phys. Rev. Lett.* **108** 245501
- [11] De Padova P, Quaresima C, Olivieri B, Perfetti P and Le Lay G 2011 Sp^2 -like hybridization of silicon valence orbitals in silicene nanoribbons *Appl. Phys. Lett.* **98** 081909
- [12] Le Lay G, Aufray B, Léandri C, Oughaddou H, Biberian J P, De Padova P, Dávila M E, Ealet B and Kara A 2009 Physics and chemistry of silicene nano-ribbons *Appl. Surf. Sci.* **256** 524–9
- [13] Kara A, Enriquez H, Seitsonen A P, Lew Yan Voon L C, Vizzini S, Aufray B and Oughaddou H 2012 A review on silicene—new candidate for electronics *Surf. Sci. Rep.* **67** 1–18
- [14] Aufray B *et al* 2010 Graphene-like silicon nanoribbons on Ag(110): a possible formation of silicone *Appl. Phys. Lett.* **96** 183102
- [15] Enriquez H, Vizzini S, Kara A, Lalmi B and Oughaddou H 2012 Silicene structures on silver surfaces *J. Phys.: Condens. Matter.* **24** 314211
- [16] Tao L, Cinquanta E, Chiappe D, Grazianetti C, Fanciulli M, Dubey M, Molle A and Akinwande D 2015 Silicene field-effect transistors operating at room temperature *Nat. Nanotechnol.* **10** 227–31
- [17] Meng L *et al* 2013 Buckled silicene formation on Ir(111) *Nano Lett.* **13** 685–90

- [18] Rachid Tchalala M *et al* 2013 Formation of one-dimensional self-assembled silicon nanoribbons on Au(110)-(2 × 1) *Appl. Phys. Lett.* **102** 083107
- [19] Liu H, Gao J and Zhao J 2013 Silicene on substrates: a way to preserve or tune its electronic properties *J. Phys. Chem. C* **117** 10353–9
- [20] Chiappe D, Scalise E, Cinquanta E, Grazianetti C, van den Broek B, Fanciulli M, Houssa M and Molle A 2014 Two-dimensional Si nanosheets with local hexagonal structure on a MoS₂ surface *Adv. Mater.* **26** 2096–101
- [21] Ali M A and Tchalala M R 2014 Chemical synthesis of silicon nanosheets from layered calcium disilicide *J. Phys.: Conf. Ser.* **491** 012009
- [22] Houssa M, Pourtois G, Afanas'ev V V and Stesmans A 2010 Can silicon behave like graphene? A first-principles study *Appl. Phys. Lett.* **97** 112106
- [23] Bhattacharya A, Bhattacharya S and Das G 2013 Exploring semiconductor substrate for silicene epitaxy *Appl. Phys. Lett.* **103** 123113
- [24] Kaloni T P, Schreckenbach G, Freund M S and Schwingenschlögl U 2016 Current developments in silicene and germanene *Phys. Status Solidi RRL* **10** 133–42
- [25] Shao Z-G, Ye X-S, Yang L and Wang C-L 2013 First-principles calculation of intrinsic carrier mobility of silicene *J. Appl. Phys.* **114** 093712
- [26] Mokkath J H and Schwingenschlögl U 2016 Tunable optical absorption in silicene molecules *J. Mater. Chem. C* **4** 7387–90
- [27] Oughaddou H, Enriquez H, Tchalala M R, Yildirim H, Mayne A J, Bendounan A, Dujardin G, Ali M A and Kara M A 2015 Silicene, a promising new 2D material *Prog. Surf. Sci.* **90** 46–83
- [28] Liu C-C, Feng W and Yao Y 2011 Quantum spin Hall effect in silicene and two-dimensional germanium *Phys. Rev. Lett.* **107** 076802
- [29] Drummond N D, Zolyomi V and Falko V I 2012 Electrically tunable band gap in silicene *Phys. Rev. B* **85** 075423
- [30] Aftab T 2017 Valleytronics and phase transition in silicone *Phys. Lett. A* **381** 935–43
- [31] Vali M, Dideban D and Moezi N 2016 Silicene field effect transistor with high on/off current ratio and good current saturation *J. Comput. Electron.* **15** 138–43
- [32] Zhu J and Schwingenschlögl U 2016 Silicene for Na-ion battery applications *2D Mater.* **3** 035012
- [33] Xu S, Fan X, Liu J, Singh D J, Jiang Q and Zheng W 2018 Adsorption of Li on single-layer silicene for anodes of Li-ion batteries *Phys. Chem. Chem. Phys.* **20** 8887–96
- [34] Mortazavi B, Dianat A, Cuniberti G and Rabczuk T 2016 Application of silicene, germanene and stanene for Na or Li ion storage: a theoretical investigation *Electrochim. Acta* **213** 865–70
- [35] Galashev A Y and Vorob'ev A S 2018 Physical properties of silicene electrodes for Li-, Na-, Mg-, and K-ion batteries *J. Solid State Electrochem.* **22** 3383–91
- [36] Li M, Li Z and Gong S-J 2018 Effect of charging on silicene with alkali metal atom adsorption *J. Phys. D: Appl. Phys.* **51** 075302
- [37] Ezawa M 2013 Spin valleytronics in silicene: quantum spin Hall-quantum anomalous Hall insulators and single-valley semimetals *Phys. Rev. B* **87** 155415
- [38] Osborne D A, Morishita T, Tawfik S A, Yayama T and Spencer M J S 2019 Adsorption of toxic gases on silicene/Ag(111) *Phys. Chem. Chem. Phys.* **21** 17521–37
- [39] Lew Yan Voon L C, Zhu J and Schwingenschlögl U 2016 Silicene: recent theoretical advances *Appl. Phys. Rev.* **3** 040802
- [40] Zhao J *et al* 2016 Rise of silicene: a competitive 2D material *Prog. Mater. Sci.* **83** 24–151
- [41] Tran N T T, Gumbs G, Nguyen D K and Lin M-F 2020 Fundamental properties of metal-adsorbed silicene: a DFT study *ACS Omega* **5** 13760–9
- [42] Jeong G H, Sasikala S P, Yun T, Lee G Y, Lee W J and Kim S O 2020 Nanoscale assembly of 2D materials for energy and environmental applications *Adv. Mater.* **32** 1907006
- [43] Gupta A, Sakthivel T and Seal S 2015 Recent development in 2D materials beyond graphene *Prog. Mater. Sci.* **73** 44–126
- [44] Bhimanapati G R *et al* 2015 Recent advances in two-dimensional materials beyond graphene *ACS Nano* **9** 11509–39
- [45] Vishnoi P, Pramoda K and Rao C N R 2019 2D elemental nanomaterials beyond graphene *ChemNanoMat* **5** 1062–91
- [46] Molle A, Grazianetti C, Tao L, Taneja D, Alam M H and Akinwande D 2018 Silicene, silicene derivatives, and their device applications *Chem. Soc. Rev.* **47** 6370–87
- [47] Lin X and Ni J 2012 Much stronger binding of metal adatoms to silicene than to graphene: a first-principles study *Phys. Rev. B* **86** 075440
- [48] Momeni M J, Mousavi-Khoshdel M and Targholi E 2017 First-principles investigation of adsorption and diffusion of Li on doped silicenes: prospective materials for lithium-ion batteries *Mater. Chem. Phys.* **192** 125–30
- [49] Gheshlagh Z H T, Beheshtian J and Mansouri S 2019 The electronic and optical properties of 3D transition metals doped silicene sheet: a DFT study *Mater. Res. Express* **6** 126326
- [50] Barhouni M, Lazaar K and Said M 2019 DFT study of electronic and optical properties of silicene functionalized with chemical groups *J. Mol. Graphics Modell.* **91** 72–9
- [51] Zhuang J, Xu X, Peleckis G, Hao W, Dou S X and Du Y 2017 Silicene: a promising anode for lithium-ion batteries *Adv. Mater.* **29** 1606716
- [52] Tritsarlis G A, Kaxiras E, Meng S and Wang E 2013 Adsorption and diffusion of lithium on layered silicon for Li-ion storage *Nano Lett.* **13** 2258–63
- [53] Osborn T H and Farajian A A 2012 Stability of lithiated silicene from first principles *J. Phys. Chem. C* **116** 22916–20
- [54] Guo G, Mao Y, Zhong J, Yuan J and Zhao H 2017 Design lithium storage materials by lithium adatoms adsorption at the edges of zigzag silicene nanoribbon: a first principle study *Appl. Surf. Sci.* **406** 161–9
- [55] Zhu J, Chroneos A and Schwingenschlögl U 2016 Silicene/germanene on MgX₂ (X = Cl, Br, and I) for Li-ion battery applications *Nanoscale* **8** 7272–7
- [56] Setiadi J, Arnold M D and Ford M J 2013 Li-ion adsorption and diffusion on two-dimensional silicon with defects: a first principles study *ACS Appl. Mater. Interfaces* **5** 10690–5
- [57] Yuan J, Tang C, Zhong J and Mao Y 2016 First-principles simulations on the new hybrid phases of germanene with alkali metal atoms coverage *Appl. Surf. Sci.* **360** 707–14
- [58] Momeni M J, Mousavi-Khoshdel M and Leisegang T 2020 Exploring the performance of pristine and defective silicene and silicene-like XSi₃ (X = Al, B, C, N, P) sheets as supercapacitor electrodes: a density functional theory calculation of quantum capacitance *Physica E* **124** 114290
- [59] Huang J, Chen H-J, Wu M-S, Liu G, Ouyang C-Y and Xu B 2013 First-principles calculation of lithium adsorption and diffusion on silicene *Chin. Phys. Lett.* **30** 017103
- [60] Seyed-Talebi S M, Kazeminezhad I and Beheshtian J 2015 Theoretical prediction of silicene; as new candidate for the anode of lithium-ion batteries *Phys. Chem. Chem. Phys.* **17** 29689–96
- [61] Gao J, Zhang J, Liu H, Zhang Q and Zhao J 2013 Structures, mobilities, electronic and magnetic properties of point defects in silicene *Nanoscale* **5** 9785–92
- [62] Yang G M, Xu Q, Fan X and Zheng W T 2018 Quantum capacitance of silicene-based electrodes from first-principles calculations *J. Phys. Chem. C* **122** 1903–12

- [63] Xu Q, Yang G M, Fan X and Zheng W T 2019 Adsorption of metal atoms on silicene: stability and quantum capacitance of silicene-based electrode materials *Phys. Chem. Chem. Phys.* **21** 4276–85
- [64] Kresse G and Joubert D 1999 From ultrasoft pseudopotentials to the projector augmented-wave method *Phys. Rev. B* **59** 1758–75
- [65] Kresse G and Furthmüller J 1996 Efficiency of *ab initio* total energy calculations for metals and semiconductors using a plane-wave basis set *Comput. Mater. Sci.* **6** 15–50
- [66] Kresse G and Furthmüller J 1996 Effective iterative schemes for *ab initio* total-energy calculations using a plane-wave basis set *Phys. Rev. B* **54** 11169–86
- [67] Blöchl P E 1994 Projector augmented-wave method *Phys. Rev. B* **50** 17953–79
- [68] Perdew J P, Burke K and Ernzerhof M 1996 Generalized gradient approximation made simple *Phys. Rev. Lett.* **77** 3865–8
- [69] Monkhorst H J and Pack J D 1976 Special points for Brillouin-zone integrations *Phys. Rev. B* **13** 5188–92
- [70] Wang Y and Li Y 2020 *Ab initio* prediction of two-dimensional Si₃C enabling high specific capacity as an anode material for Li/Na/K-ion batteries *J. Mater. Chem. A* **8** 4274–82
- [71] Paek E, Pak A J and Hwang G S 2013 A computational study of the interfacial structure and capacitance of graphene in [BMIM][PF₆] ionic liquid *J. Electrochem. Soc.* **160** A1–10
- [72] Paek E, Pak A J, Kweon K E and Hwang G S 2013 On the origin of the enhanced supercapacitor performance of nitrogen-doped graphene *J. Phys. Chem. C* **117** 5610–6
- [73] Nawaz S and Tahir M 2016 Quantum capacitance in monolayers of silicene and related buckled materials *Physica E* **76** 169–72
- [74] Zeng W, Zhang Y, Liu X, Qi L, Kang W, Fang L and Zhou M 2020 B/N-doped graphdiyne as superior supercapacitor electrode with record high quantum capacitance *Appl. Surf. Sci.* **523** 146468
- [75] Pattarapongdilok N and Parasuk V 2020 Adsorptions of lithium ion/atom and packing of Li ions on graphene quantum dots: application for Li-ion battery *Comput. Theor. Chem.* **1177** 11279
- [76] Yu Y-X 2021 High storage capacity and small volume change of potassium-intercalation into novel vanadium oxychalcogenide monolayers V₂S₂O, V₂Se₂O and V₂Te₂O: an *ab initio* DFT investigation *Appl. Surf. Sci.* **546** 149062
- [77] Yu Y-X 2013 Can all nitrogen-doped defects improve the performance of graphene anode materials for lithium-ion batteries? *Phys. Chem. Chem. Phys.* **15** 16819–27
- [78] Yu Y-X 2013 Graphenylene: a promising anode material for lithium-ion batteries with high mobility and storage *J. Mater. Chem. A* **1** 13559–66
- [79] Ali M, Pi X, Liu Y and Yang D 2017 Electronic and magnetic properties of graphene, silicene and germanene with varying vacancy concentration *AIP Adv.* **7** 045308
- [80] Hernández Cocolletzi H and Castellanos Águila J E 2018 DFT studies on the Al, B, and P doping of silicene *Superlattices Microstruct.* **114** 242–50
- [81] Hussain T, ChaKraborty S and Ahuja R 2013 Metal-functionalized silicene for efficient hydrogen storage *ChemPhysChem* **14** 3463–6
- [82] Bader R 1990 *Atoms in Molecules: A Quantum Theory* (Oxford: Oxford University Press)
- [83] Shanmugam S, Nachimuthu S and Subramaniam V 2020 The effect of edge termination on Li⁺ ion adsorption of pristine and defected graphene sheets *J. Mater. Sci.* **55** 5920–37
- [84] Sangavi S, Santhanamoorthi N and Vijayakumar S 2019 Density functional theory study on the adsorption of alkali metal ions with pristine and defected graphene sheet *Mol. Phys.* **117** 462–73